JOURNAL OF THERMOPHYSICS AND HEAT TRANSFER
Vol. 17, No. 3, July–September 2003

Refractive Index Effects on Heat Transfer in Multilayer Scattering Composite

Jian-Feng Luo,* He-Ping Tan,† and Li-Ming Ruan‡
Harbin Institute of Technology, 150001 Harbin, People's Republic of China
and
Timothy W. Tong§
George Washington University, Washington, D.C. 20052

By the use of the ray tracing method, in combination with Hottel and Sarofim's zonal method and spectral model, transient coupled radiative and conductive heat transfer in a multilayer absorbing, isotropically scattering composite with semitransparent and specular surfaces and interfaces is investigated. The specular reflectivities of all of the surfaces and interfaces are determined by Fresnel's reflective law and Snell's refractive law. For the ray tracing method, the complex total reflection problem of the multilayer composite is properly solved, and the radiative transfer coefficients (RTCs) of the multilayer composite are derived. The RTCs are used to calculate a radiative source term, and the transient energy equation is solved by the fully universal implicit discrete control volume method. Combined with extinction coefficient, conduction–radiation parameter, scattering albedo, layer thickness, and number of layers, the effects of refractive index on pure radiative and coupled radiative and conductive heat transfer are investigated. The analysis shows that, if the refractive indexes of the layers are arranged according to a specified periodical behavior along the thickness, and the other corresponding parameters of each layer are kept the same, then the temperature distribution within the composite shows a similar complex periodical behavior as well.

Nomenclature

A_{k,T_i} = fractional spectral emissive power of spectral band k at nodal temperature T_i,

$$\int_{\Delta\lambda_k} I_{\lambda,b}(T_i)\,\mathrm{d}\lambda \Big/ \left(\sigma T_i^4\right)$$

$a1_b, a2_b$ = surface, interface, or control volume of bth layer, used to define one-layer radiative intensity quotient transfer function

$b1, b2$ = surface or interface, used to define multilayer radiative intensity quotient transfer function

c_b = specific heat capacity of bth layer, $\mathrm{Jkg^{-1}\,K^{-1}}$

$\boldsymbol{F}$ = radiative intensity quotient transfer function of single-layer semitransparent medium model

$\boldsymbol{H}$ = radiative intensity quotient transfer function of multilayer semitransparent medium model

h_1, h_2 = convective heat transfer coefficient at surfaces S_1 and S_2, respectively, $\mathrm{Wm^{-2}\,K^{-1}}$

I_b = Ith node in bth layer

J_b = Jth node in bth layer

k_b = thermal conductivity of bth layer of medium, $\mathrm{Wm^{-1}\,K^{-1}}$

k_{ie} = harmonic mean thermal conductivity at interface ie of control volume i, $(\Delta x'_i + \Delta x'_{i+1})/(\Delta x'_i/k'_i + \Delta x'_{i+1}/k'_{i+1})$, $\mathrm{Wm^{-1}\,K^{-1}}$

k_{iw} = harmonic mean thermal conductivity at interface iw of control volume i, $(\Delta x'_{i-1} + \Delta x'_i)/(\Delta x'_{i-1}/k'_{i-1} + \Delta x'_i/k'_i)$, $\mathrm{Wm^{-1}\,K^{-1}}$

k'_i = thermal conductivity of ith control volume, when $i \le M_1$ and $k'_i = k_1$, when $M_1 + \cdots + M_{b-1} < i \le M_1 + \cdots + M_b$ and $k'_i = k_b$, $\mathrm{Wm^{-1}\,K^{-1}}$

L_b = thickness of bth layer, m

L_t = total thickness of composite, $L_1 + L_2 + \cdots + L_n$, m

M_b = number of control volumes of bth layer

M_t = total number of control volumes of composite, $M_1 + M_2 + \cdots + M_n$

N_b = conduction–radiation parameter of bth layer of medium, $k_b/(4\sigma T_r^3 L_t)$

n = total number of layers of the multilayer physical model (Fig. 1)

$n_{b,k}$ = spectral refractive index of bth layer

n_m = refractive index of mth element

n_0, n_{n+1} = refractive indexes of surroundings (equal to the refractive index of air n_g) (Fig. 1)

$n'_{i,k}$ = refractive index of ith control volume, when $i \le M_1$ and $n'_{i,k} = n_{1,k}$, when $M_1 + \cdots + M_{b-1} < i \le M_1 + \cdots + M_b$ and $n'_{i,k} = n_{b,k}$

P_b = interface between bth layer and $(b+1)$th layer, side of interface P_b facing toward the bth layer

$P_{b'}$ = side of interface P_b facing toward the $(b+1)$th layer

q^c, q^r = thermal conductive and radiative heat fluxes, respectively, $\mathrm{Wm^{-2}}$

q^t = total heat flux, $q^c + q^r$, $\mathrm{Wm^{-2}}$

$\tilde{q}$ = dimensionless heat flux, $q/(\sigma T_r^4)$

S_u, S_v = black surrounding surfaces, $u, v = -\infty$ or $+\infty$

S_1, S_2 = boundary surfaces (Fig. 1)

$(S_u S_v)_k$, $[S_u S_v]_k$ = ratio of radiative energy arriving at S_v to that emitted from S_u in the kth spectral band $\Delta\lambda_k$ for nonscattering and scattering media, respectively

Received 7 August 2001; revision received 21 January 2003; accepted for publication 22 January 2003.

*Graduate Student, School of Energy Science and Engineering, 92 West Dazhi Street, Harbin 150001; luo_jianfeng@yahoo.com.

†Professor, School of Energy Science and Engineering, 92 West Dazhi Street, Harbin 150001; tanheping77@yahoo.com.cn.

‡Associate Professor, School of Energy Science and Engineering, 92 West Dazhi Street, Harbin 150001; ruanlm@hope.hit.edu.cn.

§Professor, School of Engineering and Applied Science. Associate Fellow AIAA.

$(S_u V_j)_k$, $[S_u V_j]_k$ = ratio of radiative energy arriving at V_j to that emitted from S_u in the kth spectral band $\Delta\lambda_k$ for nonscattering and scattering media, respectively
$S_{-\infty}$, $S_{+\infty}$ = left and right black surfaces representing the surroundings (Fig. 1)
T_{g1}, T_{g2} = gas temperature for convection at $x = 0$ and L_t, respectively, K
T_r = reference temperature, K
T_{S_1}, T_{S_2} = temperatures of boundary surfaces S_1 and S_2, respectively, K
T_0 = uniform initial temperature, K
$T_{-\infty}$, $T_{+\infty}$ = temperatures of black surfaces $S_{-\infty}$ and $S_{+\infty}$, respectively, K (Fig. 1)
t = physical time, s
t^* = dimensionless time, $4\sigma T_r^3 t/(\rho_1 c_1 L_t)$
V_{I_b} = Ith control volume of bth layer, $I = 1$ to M_b
V_i = ith control volume, $i = M_1 + \cdots + M_{b-1} + I_b$
$(V_i V_j)_k$, $[V_i V_j]_k$ = ratios of radiative energy arriving at V_j to that emitted from V_i in the kth spectral band $\Delta\lambda_k$ for nonscattering and scattering media, respectively
X = dimensionless coordinate in direction across layer, $X = x/L_t$
x_i, y_i, z_i = geometrical progressions used in tracing radiative intensity
$x_{I_b}^A$ = distance between interface A and the boundary I_b of control volume V_{I_b}, m
$\alpha_{b,k}$ = kth spectral band absorption coefficient of bth layer of medium, m^{-1}
$\Gamma(\theta)$ = transfer quotient of radiative intensity to control volume or surface [Eq. (7)]
$\gamma(\theta)_{bo}$ = transmissivity of radiative intensity propagating from layer b to layer o at angle θ, $1 - \rho(\theta)_{bo}$
Δt = time interval, s
Δx_b = control volume thickness of bth layer, m
$\Delta x_i'$ = thickness of ith control volume, m, when $i \le M_1$ and $\Delta x_i' = \Delta x_1$, when $M_1 + \cdots + M_{b-1} < i \le M_1 + \cdots + M_b$, where $1 < b \le n$ and $\Delta x_i' = \Delta x_b$
$(\delta x)_{ie}$ = distance between nodes i and $i+1$, $(\Delta x_i' + \Delta x_{i+1}')/2$, m (Fig. 1)
$(\delta x)_{iw}$ = distance between i and $i-1$, $(\Delta x_i' + \Delta x_{i-1}')/2$, m (Fig. 1)
$\eta_{i,k}$ = $1 - \omega_{i,k}'$
Θ = dimensionless temperature, T/T_r
θ = incident angle of mth element, rad
θ_b = refractive angle in bth layer, $\arcsin(\sin\theta n_m/n_b)$, rad
θ_{ba} = arrangement of critical angles θ_{ba}' from small to big, where $a = 0$ to $n+1$
θ_{ba}' = critical angle; if $n_b > n_a$, $\theta_{ba}' = \arcsin(n_a/n_b)$, else $\theta_{ba}' = (\pi/2)$, where $a = 0$ to $n+1$
$\kappa_{b,k}$ = kth spectral band extinction coefficient of bth layer of medium, $\alpha_{b,k} + \sigma_{s,b,k}$, m^{-1}
μ_b = $\cos\theta_b$
ρ_b = density of bth layer of medium, kg/m^3
$\rho(\theta)_{bo}$ = reflectivity of radiative intensity going from layer b to layer o at angle θ
σ = Stefan–Boltzmann constant, $Wm^{-2}\ K^{-4}$
$\sigma_{s,b,k}$ = kth spectral band scattering coefficient of bth layer of medium, m^{-1}
$\tau_{b,k}$ = kth spectral band optical thickness of bth layer, $\kappa_{b,k} L_b$
Φ_i^r = radiative heat source term of control volume i
φ_o = refractive angle in oth layer, $\arcsin(n_b/n_o \sin\theta_b)$
$\omega_{b,k}$ = kth spectral band scattering albedo of bth layer, $\sigma_{s,b,k}/\kappa_{b,k}$
$\omega_{i,k}'$ = kth spectral band scattering albedo of ith control volume, when $i \le M_1$ and $\omega_{i,k}' = \omega_{1,k}$, when $M_1 + \cdots + M_{b-1} < i \le M_1 + \cdots + M_b$, where $1 < b \le n$ and $\omega_{i,k}' = \omega_{b,k}$

Subscripts

a = layer index, absorption quotient, $a = 1$–n
b = layer index, $b = 1$–n
bo = radiative intensity propagating from layer b to layer o
c = cth layer, either b or o layer
g = gas (air)
iw, ie = left and right interfaces of ith control volume
k = relative to kth spectral band
o = oth layer, either $b-1$ or $b+1$ layer
S_1, S_2 = relative to S_1 and S_2
$t - t$ = refers to a composite with semitransparent surfaces
$-\infty$, $+\infty$ = relative to $S_{-\infty}$ and $S_{+\infty}$
$/\!/$, $\perp$ = relative to component for parallel and perpendicular polarization, respectively

Superscripts

m = time step
s = specular reflection
$*$ = normalized values

Introduction

COUPLED radiative and conductive heat transfer in semitransparent media is pervasive in engineering applications, such as ceramic components for high-temperature use, tempering of glass windows, and insulating techniques for the protection of aeroengines. The refractive index plays an important role in coupled radiative and conductive heat transfer. On one hand, the emission of a medium is proportional to the square of the refractive index. On the other hand, the reflection and refraction at a semitransparent interface, which are determined by Fresnel's reflective law and Snell's refractive law, are intimately related to the refractive indexes on both sides of the interface. If the refractive index of the medium on one side of an interface is much larger than that on the other side, the reflected energy at the interface becomes very large, as compared to the case where the two refractive indexes are not as mismatched. Generally, the larger the refractive index of one layer is, the more uniform the temperature distribution for pure radiation is therein. Differing from diffuse reflectivity, specular reflectivity of a semitransparent interface is dependent on ray incident angle.

Many researchers have investigated the effects of refractive index on heat transfer. Siegel and Spuckler investigated the effects of refractive index on radiative heat transfer[1,2] and coupled heat transfer[3,4,5] with diffuse reflection. Considering refractive index to be larger than unity, Liu and Dougherty,[6] Crosbie and Shieh,[7] Schwander et al.,[8] and Tan and Lallemand[9] investigated the effects of Fresnel boundary reflection. Su and Sutton[10] studied transient coupled radiative and conductive heat transfer in a nongray electromagnetic window with semitransparent specular surfaces and considered the refractive index to be a function of temperature and wavelength. Abulwafa[11] recently studied coupled radiative and conductive heat transfer in an anisotropically scattering layer with semitransparent, specular, or diffuse surfaces. Siegel[12] investigated the effects of the refractive index and specular and diffuse reflection on radiative heat transfer in an isothermal layer with semitransparent surfaces.

For coupled radiative and conductive heat transfer in a multilayer composite, reflection, total reflection, and interactions among all layers become very complex with an increasing number of layers. Early in 1986, Tsai and Nixon[13] and Timoshenko and Trenev[14] investigated the transient coupled radiative and conductive heat transfer in a multilayer absorbing composite, but Fresnel's reflective law and Snell's refractive law were not employed in the two papers to determine interface reflectivity. However, in 1993, Siegel and Spuckler[2] studied the effects of the refractive index on pure radiative heat transfer in a multilayer absorbing, isotropically scattering composite with semitransparent diffuse surfaces and interfaces; and the diffuse reflectivities of all of the surfaces and interfaces were

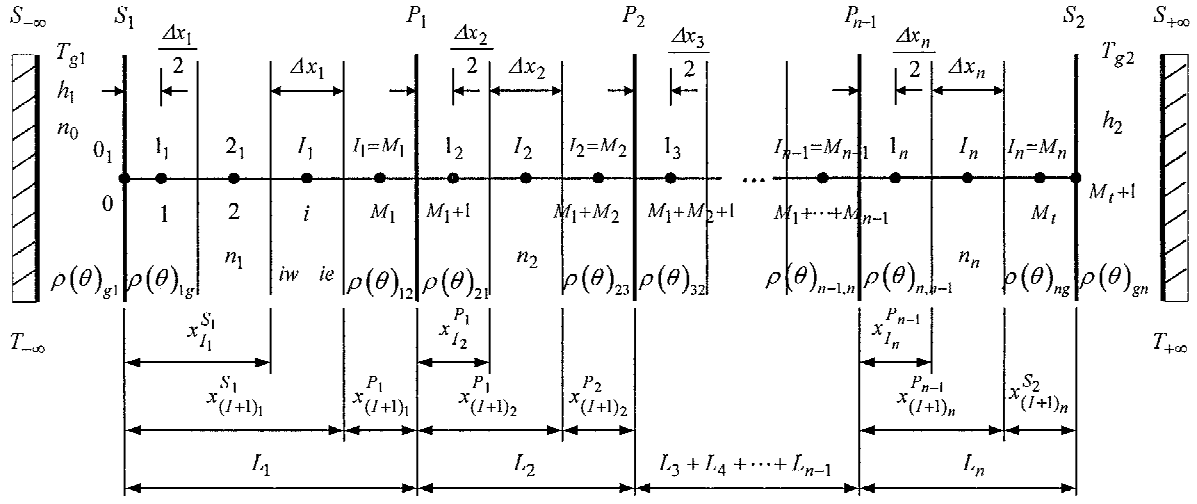

Fig. 1 Physical model of *n*-layer semitransparent composite medium with semitransparent specular surfaces and interfaces.

obtained from Fresnel's reflective law and Snell's refractive law under the assumption that each bit of roughness acts as a smooth facet and by integration of the reflected energy over all incident directions.

By the use of the ray-tracing/node-analyzing method, in combination with Hottel and Sarofim's zonal method,[15] transient coupled heat transfer in a two-layer absorbing, isotropically scattering composite was investigated, and the two-layer composite was considered with two semitransparent surfaces,[16] two opaque surfaces,[17] and one opaque surface and one semitransparent surface.[18] Considering the effects of Fresnel's reflection and Snell's refraction, Tan et al.[19] and Luo et al.[20] studied transient coupled heat transfer in a three-layer scattering composite with specular semitransparent surfaces[19] and opaque surfaces.[20]

Based on Refs. 19 and 20, in the present study, the effects of the refractive index on transient coupled heat transfer and pure radiative heat transfer in a multilayer absorbing, isotropically scattering composite with semitransparent specular surfaces and interfaces are investigated. The effects of the extinction coefficient, scattering albedo, conduction–radiation parameter, and convection–radiation boundary conditions on heat transfer are studied as well. The differences between the present results and those of Ref. 2 are as follows: In this paper, all of the surfaces and interfaces are semitransparent and specular, whereas, on the contrary, in Ref. 2 the surfaces and interfaces are semitransparent and diffuse. Transient coupled radiative–conductive heat transfer and pure radiative heat transfer are studied simultaneously in this paper, but only pure radiative heat transfer is investigated in Ref. 2. The diffuse reflectivity of a semitransparent interface is suitable for characterizing the radiative energy coming from the whole hemispherical space, and the total reflection is considered in the reflectivity formula. In contrast, the specular reflectivity of a semitransparent interface is suitable for characterizing the radiative intensity coming from one direction, and total reflection occurs when the incident angle is greater than the critical angle.

As used in Ref. 12, for unpolarized incidence, the radiative intensity can be divided into two equal, parallel, and perpendicular parts. With correspondence to the two parts, the reflectivity of a semitransparent interface is classified into two parts also, as shown in Appendix A. For a multilayer composite, the discretionary arrangement of refractive index magnitude among all layers makes total reflection in the composite very complex, and, in this paper, a proper method has been deduced to solve this problem.

Physical Model and Discrete Governing Equation

Physical Model

As shown in Fig. 1, a composite composed of n absorbing, isotropically scattering layers with different optical and thermal properties is located between two black surfaces $S_{-\infty}$ and $S_{+\infty}$. The two boundary surfaces S_1 and S_2, and the interfaces, P_1, P_2, ..., and P_{n-1}, of the composite are semitransparent and specular. The thickness, refractive index, and extinction coefficient of each layer are L_b, n_b and κ_b, respectively, and the refractive indexes of surrounding medium are n_0 and n_{n+1}. Along the thickness direction, the n layers are divided into M_1, M_2, ..., and M_n control volumes, respectively, and I_b is used to denote the Ith node in the bth layer. The total numbers of nodes are $M_t + 2$ $(0, 1, \ldots, M_t + 1)$ with node 0 locating S_1 and node $M_t + 1$ locating S_2. For convenience, all of the nodes are denoted by i as well, and if $b = 1$, then $i = I_1$. Otherwise, if $1 < b \le n$, then, $i = M_1 + M_2 + \cdots + M_{b-1} + I_b$ (refer to Fig. 1). As shown in Fig. 1, the center point of each control volume is chosen as the node. Thus, except for node 0 and node $M_t + 1$, the distance between two neighboring nodes, node i and node $i + 1$, is $(\Delta x_i' + \Delta x_{i+1}')/2$, but the distance between nodes 0 and 1 is $\Delta x_1'/2$ $(= \Delta x_1/2)$, and that between node M_t and node $M_t + 1$ is $\Delta x_{M_t}'/2$ $(= \Delta x_n/2)$.

The variation of κ_b, n_b, α_b, $\sigma_{s,b}$, and ω_b with respect to wavelength is approximately expressed by spectral bands.[16]

Discrete Governing Equation and Boundary Condition

The fully implicit discrete governing equation of ith control volume in the bth layer is[16]

$$\rho_b c_b \Delta x_b \frac{T_i^{m+1} - T_i^m}{\Delta t} = \frac{k_{ie}^{m+1}\left(T_{i+1}^{m+1} - T_i^{m+1}\right)}{(\delta x)_{ie}} - \frac{k_{iw}^{m+1}\left(T_i^{m+1} - T_{i-1}^{m+1}\right)}{(\delta x)_{iw}} + \Phi_i^{r,m+1} \tag{1}$$

With reference to the expression of a radiative source term for a two-layer composite with semitransparent surfaces,[16] the expression of a radiative source term of control volume i for a multilayer composite can be expressed as $\Phi_i^r = q_{iw}^r - q_{ie}^r = q_{(i-1)e}^r - q_{ie}^r$, where $q_{iw}^r = q_{(i-1)e}^r$ represents the net radiative energy passing through the left boundary of control volume i, and q_{ie}^r represents that passing through the right boundary of control volume i. If $1 \le i \le M_t$, then q_{ie}^r can be expressed as[16]

$$q_{ie}^r = \sigma \sum_{k=1}^{NB} \left(\sum_{j=i+1}^{M_t} \left\{ \left[S_{-\infty} V_j \right]_{k,t-t}^s A_{k,T_{-\infty}} T_{-\infty}^4 - n'^2_{j,k} \left[V_j S_{-\infty} \right]_{k,t-t}^s A_{k,T_j} T_j^4 \right\} + \sum_{l=1}^{i} \sum_{j=i+1}^{M_t} \left\{ n'^2_{l,k} \left[V_l V_j \right]_{k,t-t}^s A_{k,T_l} T_l^4 \right.$$

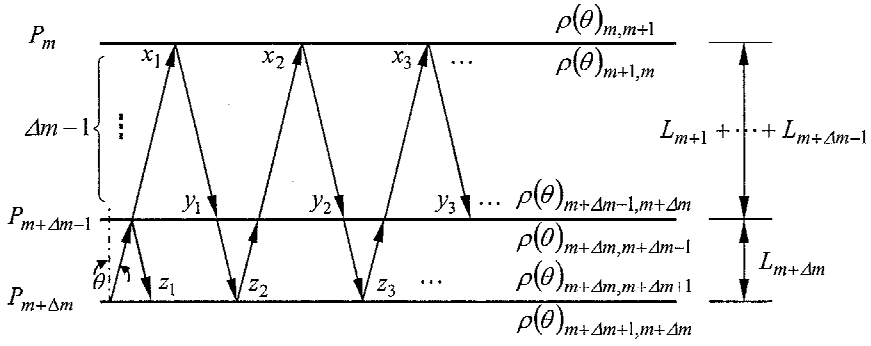

Fig. 2 Multilayer radiative intensity transfer model.

$$-n'^2_{j,k}[V_jV_l]^s_{k,t-t}A_{k,T_j}T_j^4\Big\}$$

$$+\sum_{l=1}^{i}\Big\{n'^2_{l,k}[V_lS_{+\infty}]^s_{k,t-t}A_{k,T_l}T_l^4-[S_{+\infty}V_l]^s_{k,t-t}A_{k,T_{+\infty}}T^4_{+\infty}\Big\}$$

$$+\Big\{\big[S_{-\infty}S_{+\infty}\big]^s_{k,t-t}A_{k,T_{-\infty}}T^4_{-\infty}-[S_{+\infty}S_{-\infty}]^s_{k,t-t}A_{k,T_{+\infty}}T^4_{+\infty}\Big\}\Bigg) \tag{2}$$

The balance of heat transfer on surfaces (without coatings) of the composite only relates to inner conduction and external convection. Taking S_1 as an example, the boundary condition is

$$-k_1\left.\frac{\partial T}{\partial x}\right|_{x=0}=h_1\big(T_{g1}-T_{S_1}\big)$$

The two nodes, 0 and 1, are employed to discretize the left term of the preceding equation, and so the discrete boundary condition of the surface is

$$(2k_1/\Delta x_1)\big(T_{S_1}-T_1\big)=h_1\big(T_{g1}-T_{S_1}\big) \tag{3}$$

However, the temperature of node 1 in Eq. (3), T_1, must satisfy the energy conservation equation (1), which contains the radiative source term Φ_i^r of the node 1 (control volume 1). Thus, the effect of absorbed radiative energy by node 1 (control volume 1) in the boundary equation (3), has been considered. The discrete boundary condition of S_2 is similar to Eq. (3).

Radiative Transfer Coefficients (RTCs) of n-Layer Composite with Semitransparent Specular Surfaces and Interfaces

The radiative transfer for this case can be classified into two subprocesses[21]: 1) The first is an emitting-attenuating-reflecting sub process. Only emission and attenuation of the medium and reflection from the interface are considered, and the radiative transfer coefficients (RTCs) are denoted by $(V_iV_j)^s_{k,t-t}$, etc. 2) The second is an absorbing-scattering subprocess. For an isotropically scattering medium, the RTCs are denoted by $[V_iV_j]^s_{k,t-t}$, etc.

All of the RTCs of the emitting-attenuating-reflecting subprocess satisfy the following relationships:

$$\begin{aligned}
n^2_{a,k}\big(V_{I_a}V_{I_b}\big)^s_{k,t-t}&=n^2_{b,k}\big(V_{I_b}V_{I_a}\big)^s_{k,t-t}\\
n^2_{a,k}\big(V_{I_a}S_{+\infty}\big)^s_{k,t-t}&=\big(S_{+\infty}V_{I_a}\big)^s_{k,t-t}\\
\big(S_{-\infty}V_{I_b}\big)^s_{k,t-t}&=n^2_{b,k}\big(V_{I_b}S_{-\infty}\big)^s_{k,t-t}\\
(S_{-\infty}S_{+\infty})^s_{k,t-t}&=(S_{+\infty}S_{-\infty})^s_{k,t-t}
\end{aligned} \tag{4}$$

where subscripts a and b denote the ath and the bth layers, respectively, and $a, b = 1$–n.

Radiative Intensity Transfer Model for Emitting-Attenuating-Reflecting Subprocess

Single-layer and multilayer radiative intensity quotient transfer functions are used in this paper to trace the radiative intensity transferring in the n-layer composite. For convenience, in the following explanation, the notation for the two sides of a semitransparent interface is specified as follows: Let P_m be the interface between the mth and the $(m+1)$th layers. The side of that interface that faces the mth layer is denoted as P_m. The side of that interface that faces the $(m+1)$th layer is denoted as $P_{m'}$. Thus, the symbol P_m denotes not only interface P_m but also the side of that interface that faces the mth layer.

Single-layer radiative intensity quotient transfer functions, expressed by the symbol $\boldsymbol{F}^{a2_b}_{a1_b,k}$, are presented in Appendix B. The multilayer radiative intensity quotient transfer functions, as shown in Fig. 2, are expressed by the symbol $\boldsymbol{H}^{b2}_{b1,m+1\sim m+\Delta m,k}$, which means the quotient of the spectral radiative intensity arrived at interface $b2$ (representing $P_{m'}$, $P_{m+1'}$, $P_{m+\Delta m-1}$, or $P_{m+\Delta m}$) to that emitted by interface $b1$ (representing $P_{m'}$ or $P_{m+\Delta m}$) for the kth spectral band after the energy transferring once within the multilayer model. The subscript $m+1\sim m+\Delta m$ denotes that the multilayer model is composed of the layers from the $(m+1)$th layer to the $(m+\Delta m)$th layer. The process wherein radiative intensity is reflected and attenuated within the model for so many times that it finally becomes zero is defined as transferring once. (See Ref. 20, which has a more detailed explanation of this process.)

There are six kinds of multilayer radiative intensity quotient transfer functions: $\boldsymbol{H}^{P_{m'}}_{P_{m'},m+1\sim m+\Delta m,k}$, $\boldsymbol{H}^{P_{m+1'}}_{P_{m'},m+1\sim m+\Delta m,k}$, $\boldsymbol{H}^{P_{m+\Delta m}}_{P_{m'},m+1\sim m+\Delta m,k}$, $\boldsymbol{H}^{P_{m+\Delta m}}_{P_{m+\Delta m},m+1\sim m+\Delta m,k}$, $\boldsymbol{H}^{P_{m+\Delta m-1}}_{P_{m+\Delta m},m+1\sim m+\Delta m,k}$, and $\boldsymbol{H}^{P_{m'}}_{P_{m+\Delta m},m+1\sim m+\Delta m,k}$. Take $\boldsymbol{H}^{P_{m'}}_{P_{m+\Delta m},m+1\sim m+\Delta m,k}$ and $\boldsymbol{H}^{P_{m+\Delta m}}_{P_{m+\Delta m},m+1\sim m+\Delta m,k}$ as examples for the purposes of illustration of the deductive process of the multilayer radiative intensity quotient transfer function. For convenience, subscript k is omitted. As shown in Fig. 2, assume that $P_{m+\Delta m}$ emits radiative intensity at angle θ, and then we can trace it as follows.

1) After the radiative intensity transfers once within the $(m+\Delta m)$th layer, $\boldsymbol{F}^{P_{m+\Delta m-1'}}_{P_{m+\Delta m}}\gamma(\theta)_{m+\Delta m,m+\Delta m-1}$, part of it traverses $P_{m+\Delta m-1}$ and enters the top $\Delta m-1$ layers. Then after transferring once within the $\Delta m-1$ layers, the part of the radiative intensity reaching $P_{m'}$ for the first time is

$$x_1=\boldsymbol{F}^{P_{m+\Delta m-1'}}_{P_{m+\Delta m}}\gamma(\theta)_{m+\Delta m,m+\Delta m-1}\boldsymbol{H}^{P_{m'}}_{P_{m+\Delta m-1},m+1\sim m+\Delta m-1}$$

and that reaching $P_{m+\Delta m-1}$ for the first time is

$$y_1=\boldsymbol{F}^{P_{m+\Delta m-1'}}_{P_{m+\Delta m}}\gamma(\theta)_{m+\Delta m,m+\Delta m-1}\boldsymbol{H}^{P_{m+\Delta m-1}}_{P_{m+\Delta m-1},m+1\sim m+\Delta m-1}$$

2) A fraction, $\gamma(\theta)_{m+\Delta m-1,m+\Delta m}$, of the radiative intensity that reaches $P_{m+\Delta m-1}$ will enter the $(m+\Delta m)$th layer. Then, after transferring once within the layer, a quotient, $\gamma(\theta)_{m+\Delta m-1,m+\Delta m}\boldsymbol{F}^{P_{m+\Delta m-1'}}_{P_{m+\Delta m-1'}}\gamma(\theta)_{m+\Delta m,m+\Delta m-1}$, will traverse

$P_{m+\Delta m-1}$ and enter the top $\Delta m-1$ layers. Then, after transferring once within the $\Delta m-1$ layers, the quotient of the radiative intensity reaching $P_{m'}$ to that reaching $P_{m+\Delta m-1}$ is

$$\gamma(\theta)_{m+\Delta m-1,m+\Delta m}\boldsymbol{F}^{P_{m+\Delta m-1'}}_{P_{m+\Delta m-1'}}\gamma(\theta)_{m+\Delta m,m+\Delta m-1}\times\boldsymbol{H}^{P_{m'}}_{P_{m+\Delta m-1},m+1\sim m+\Delta m-1}$$

and that reaching $P_{m+\Delta m-1}$ to that reaching $P_{m+\Delta m-1}$ is

$$\beta_2=\gamma(\theta)_{m+\Delta m-1,m+\Delta m}\boldsymbol{F}^{P_{m+\Delta m-1'}}_{P_{m+\Delta m-1'}}\gamma(\theta)_{m+\Delta m,m+\Delta m-1}\times\boldsymbol{H}^{P_{m+\Delta m-1}}_{P_{m+\Delta m-1},m+1\sim m+\Delta m-1}\ (<1)$$

Thus, after the fraction y_1, derived in step 1, experiences the preceding process, the quotient of the radiative intensity reaching $P_{m'}$ to that emitted by $P_{m+\Delta m}$ for the second time is

$$x_2=y_1\gamma(\theta)_{m+\Delta m-1,m+\Delta m}\boldsymbol{F}^{P_{m+\Delta m-1'}}_{P_{m+\Delta m-1'}}\gamma(\theta)_{m+\Delta m,m+\Delta m-1}\times\boldsymbol{H}^{P_{m'}}_{P_{m+\Delta m-1},m+1\sim m+\Delta m-1}$$

and that reaching $P_{m+\Delta m-1}$ to that emitted by $P_{m+\Delta m}$ for the second time is

$$y_2=y_1\beta_2$$

3) When step 2 is repeated for quotient y_2, the quotient of the radiative intensity reaching $P_{m'}$ to that emitted by $P_{m+\Delta m}$ for the third time is

$$x_3=y_2\gamma(\theta)_{m+\Delta m-1,m+\Delta m}\boldsymbol{F}^{P_{m+\Delta m-1'}}_{P_{m+\Delta m-1'}}\gamma(\theta)_{m+\Delta m,m+\Delta m-1}\times\boldsymbol{H}^{P_{m'}}_{P_{m+\Delta m-1},m+1\sim m+\Delta m-1}$$

and that reaching $P_{m+\Delta m-1}$ to that emitted by $P_{m+\Delta m}$ for the third time is

$$y_3=y_2\beta_2$$

Thus, repeating the tracing process for quotient y_i again and again until it finally attenuates to 0, the total quotient of the radiative intensity finally reaching $P_{m'}$ to that emitted by $P_{m+\Delta m}$ can be calculated,

$$\boldsymbol{H}^{P_{m'}}_{P_{m+\Delta m},m+1\sim m+\Delta m}=\sum_{i=1}^{\infty}x_i=x_1+\frac{x_2}{(1-\beta_2)}\qquad(5a)$$

where $x_2, x_3, \ldots,$ is an infinite geometric progression with common ratio $\beta_2(<1)$.

In a similar way, the other multilayer radiative intensity quotient transfer function, $\boldsymbol{H}^{P_{m+\Delta m}}_{P_{m+\Delta m},m+1\sim m+\Delta m}$, can be deduced:

$$\boldsymbol{H}^{P_{m+\Delta m}}_{P_{m+\Delta m},m+1\sim m+\Delta m}=\sum_{i=1}^{\infty}z_i=z_1+\frac{z_2}{(1-\beta_2)}\qquad(5b)$$

where $z_1=\boldsymbol{F}^{P_{m+\Delta m}}_{P_{m+\Delta m}}$, and $z_2=\boldsymbol{F}^{P_{m+\Delta m-1'}}_{P_{m+\Delta m}}\gamma(\theta)_{m+\Delta m,m+\Delta m-1}\boldsymbol{H}^{P_{m+\Delta m-1}}_{P_{m+\Delta m-1},m+1\sim m+\Delta m-1}\gamma(\theta)_{m+\Delta m-1,m+\Delta m}\boldsymbol{F}^{P_{m+\Delta m}}_{P_{m+\Delta m-1'}}$.

Equation (5) contains $\boldsymbol{H}^{P_{m+\Delta m-1}}_{P_{m+\Delta m-1},m+1\sim m+\Delta m-1}$ and $\boldsymbol{H}^{P_{m'}}_{P_{m+\Delta m-1},m+1\sim m+\Delta m-1}$, and so it is an iterative formula. In fact, calculation should begin from the $(m+1)$th layer, that is, $\boldsymbol{H}^{P_{m'}}_{P_{m+1}}=\boldsymbol{F}^{P_{m'}}_{P_{m+1'}}$ and $\boldsymbol{H}^{P_{m+1}}_{P_{m+1}}=\boldsymbol{F}^{P_{m+1}}_{P_{m+1}}$ are calculated first. Then, based on these two equations and combined with the single-layer radiative intensity quotient transfer functions of the $(m+2)$th layer, $\boldsymbol{H}^{P_{m+2}}_{P_{m+2},m+1\sim m+2}$ and $\boldsymbol{H}^{P_{m'}}_{P_{m+2},m+1\sim m+2}$ can be deduced from Eq. (5). Then, further based on these two equations and combined with the single-layer radiative intensity quotient transfer functions of the $(m+3)$th layer, $\boldsymbol{H}^{P_{m+3}}_{P_{m+3},m+1\sim m+3}$ and $\boldsymbol{H}^{P_{m'}}_{P_{m+3},m+1\sim m+3}$ can be calculated from Eq. (5). In the end, we can obtain the values of $\boldsymbol{H}^{P_{m'}}_{P_{m+\Delta m},m+1\sim m+\Delta m,k}$ and $\boldsymbol{H}^{P_{m+\Delta m}}_{P_{m+\Delta m},m+1\sim m+\Delta m}$; $\gamma(\theta)$ and $\rho(\theta)$ in Eq. (5) are functions of the polarized components, as shown in Appendix A.

In a similar manner, the other multilayer radiative intensity quotient transfer functions can be calculated. For simplicity, those expressions are omitted.

RTCs of *n*-Layer Composite for Emitting-Attenuating-Reflecting Subprocess

It is very convenient to trace the radiative intensity transferring in the n-layer composite by the use of the multilayer radiative intensity quotient functions. Take $(V_{I_b}S_{+\infty})^{s}_{k,t-t}$ as an example to illustrate the deductive process of the RTCs. For convenience, subscript k is omitted in the following.

As shown in Fig. 3, after the radiative intensity that is emitted by V_{I_b} transfers once within the bth layer, the portions of it reaching P_b and $P_{b-1'}$ for the first time are $x_1=\boldsymbol{F}^{P_b}_{V_{I_b}}$ and $z_1=\boldsymbol{F}^{P_{b-1'}}_{V_{I_b}}$, respectively. Then these two portions traverse P_b and P_{b-1} and transfer in the n-layer composite until they attenuate to zero. When the two transfer processes are traced, the total quotient reaching S_2 to that emitted by V_{I_b} can be obtained, in which only the $\gamma(\theta)_{ng}$ portion will traverse S_2 and be absorbed by $S_{+\infty}$. Take quotient $x_1=\boldsymbol{F}^{P_b}_{V_{I_b}}$ to illustrate the transfer process in the n layers.

1) A fraction, $\gamma(\theta)_{b,b+1}$, of the radiative intensity x_1 will penetrate P_b to enter into the following layers from the $(b+1)$th layer to the nth layer. Then, after it transfers once therein, the quotient, $y_1=x_1\gamma(\theta)_{b,b+1}\boldsymbol{H}^{S_2}_{P_{b'},b+1\sim n}$, arrives at S_2, of the radiative intensity, which is emitted by V_{I_b}, and after transferring once within the bth layer, reaches P_b for the first time, and the quotient of that arriving at $P_{b'}$ to that emitted by V_{I_b} and reaching P_b after it transfers once within the bth layer is $x_1\gamma(\theta)_{b,b+1}\boldsymbol{H}^{P_{b'}}_{P_{b'},b+1\sim n}$. Then, a fraction, $\gamma(\theta)_{b+1,b}$, of $x_1\gamma(\theta)_{b,b+1}\boldsymbol{H}^{P_{b'}}_{P_{b'},b+1\sim n}$ traverses P_b and enters the top layers from the first layer to the bth layer. After transferring once within the first to the bth layers, the quotient of the radiative intensity reaching P_b to that emitted by V_{I_b} and reaching P_b after it transfers once within the bth layer for the second time is $x_2=x_1\beta_3$, where $\beta_3=\gamma(\theta)_{b,b+1}\boldsymbol{H}^{P_{b'}}_{P_{b'},b+1\sim n}\gamma(\theta)_{b+1,b}\boldsymbol{H}^{P_b}_{P_{b,1\sim b}}$ (<1).

2) The fraction represented by x_2 repeats step 1. Then the quotient fraction of the radiative intensity arriving S_2 to that emitted by V_{I_b} and reaching P_b after it transfers once within the bth layer for the second time is

$$y_2=x_2\gamma(\theta)_{b,b+1}\boldsymbol{H}^{S_2}_{P_{b'},b+1\sim n}$$

and that reaching P_b for the third time is $x_3=x_2\beta_3$.

Hence, by tracing the transfer process again and again until the radiative intensity attenuates to 0, the total fraction arriving at S_2 is

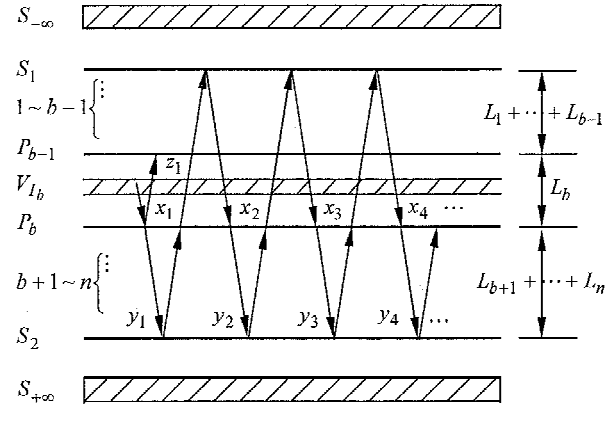

Fig. 3 RTC $(V_{I_b}S_{+\infty})^{s}_{k,t-t}$ ray trajectories.

the sum of a geometric progression,

$$\sum_{i=1}^{\infty} y_i = \frac{y_1}{(1-\beta_3)}$$

where $\beta_3(<1)$ is the common ratio of the geometric progression. Only a fraction $\gamma(\theta)_{ng}$ of

$$\sum_{i=1}^{\infty} y_i$$

traverses S_2 and is absorbed by $S_{+\infty}$. Thus, finally, the fraction absorbed by $S_{+\infty}$ of the original portion x_1 is

$$\Gamma_1(\theta) = \frac{y_1}{1-\beta_3}\gamma(\theta)_{ng}$$

$$= \frac{\boldsymbol{F}_{V_{I_b}}^{P_b}\gamma(\theta)_{b,b+1}\boldsymbol{H}_{P_{b'},b+1\sim n}^{S_2}}{1-\gamma(\theta)_{b,b+1}\boldsymbol{H}_{P_{b'},b+1\sim n}^{P_{b'}}\gamma(\theta)_{b+1,b}\boldsymbol{H}_{P_b,1\sim b}^{P_b}}\gamma(\theta)_{ng} \qquad (6a)$$

Note that Eq. (6a) is suitable for $b \neq n$. If $b=n$, then $\Gamma_1 = \boldsymbol{F}_{V_{I_n}}^{S_2}\gamma(\theta)_{ng}$.

Similarly, when the other radiative intensity quotient, $z_1 = \boldsymbol{F}_{V_{I_b}}^{P_{b-1'}}$ is traced and transferred once in the n layers, the other radiative intensity quotient transfer function, the fraction of z_1 absorbed by $S_{+\infty}$, is

$$\Gamma_2(\theta) = \frac{\boldsymbol{F}_{V_{I_b}}^{P_{b-1'}}\gamma(\theta)_{b,b-1}\boldsymbol{H}_{P_{b-1},1\sim b-1}^{P_{b-1}}\gamma(\theta)_{b-1,b}\boldsymbol{H}_{P_{b-1'},b\sim n}^{S_2}}{1-\gamma(\theta)_{b,b-1}\boldsymbol{H}_{P_{b-1},1\sim b-1}^{P_{b-1}}\gamma(\theta)_{b-1,b}\boldsymbol{H}_{P_{b-1'},b\sim n}^{P_{b-1'}}}\gamma(\theta)_{ng} \qquad (6b)$$

Equation (6b) is applicable to $b \neq 1$. If $b=1$, then $\Gamma_2 = 0$.

Finally, the total quotient of the radiative intensity absorbed by $S_{+\infty}$ to that emitted by V_{I_b} is

$$\Gamma(\theta) = \Gamma_1(\theta) + \Gamma_2(\theta) \qquad (7)$$

The values of $\Gamma(\theta)$ are different, corresponding to the two parallel and perpendicular components. Thus, for unpolarized incidence, the total quotient absorbed by $S_{+\infty}$ can be expressed as $[\Gamma(\theta)_{//}+\Gamma(\theta)_{\perp}]/2$. Integrating this expression over the whole hemispherical space gives $(V_{I_b}S_{+\infty})_{k,t-t}^{s}$. Equation (7) is a discontinuous function over the whole hemispherical space because of total reflection, $\rho(\theta)=1$, so that the following method is used to overcome this difficulty:

1) Solve for the critical angles of the bth layer vs other layers and the surroundings. If $n_b > n_a$ ($a=0$ to $n+1$), then $\theta'_{ba} = \arcsin(n_a/n_b)$. Otherwise, if $n_b \leq n_a$, no total reflection occurs, and $\theta'_{ba} = \pi/2$. After doing this, $n+2$ critical angles, $\theta'_{b0}, \theta'_{b1}, \theta'_{b2}, \ldots, \theta'_{bn}$, and $\theta'_{b(n+1)}$ are obtained, where θ'_{bb} must equal the biggest angle $\pi/2$.

2) Arrange these angles from smallest to largest, and assume that the rearranged array is $\theta_{b(-1)}(=0) < \theta_{b0} \leq \theta_{b1} \leq \theta_{b2} \leq \cdots \leq \theta_{b(n+1)}$, where $\theta_{b(n+1)}$ must equal $\pi/2$.

That is, the whole hemispherical space is divided into $n+2$ intervals separated by the critical angles, $[\theta_{b(-1)}, \theta_{b0}]$, $[\theta_{b0}, \theta_{b1}], \ldots,$ and $[\theta_{bn}, \theta_{b(n+1)}]$, and, within any interval, the function Γ becomes continuous. Thus,

$$\left(V_{I_b}S_{+\infty}\right)_{k,t-t}^{s} = \sum_{i=-1}^{n}\int_{\theta_{bi}}^{\theta_{b(i+1)}}[\Gamma(\theta)_{//}+\Gamma(\theta)_{\perp}]\cos\theta\sin\theta\,\mathrm{d}\theta \qquad (8)$$

What needs to be emphasized in Eq. (8) is that the criterion for total reflection to occurr, as discussed in Appendix A, must be used when this equation is integrated. Similarly, the other RTCs can be determined.

RTCs of *n*-Layer Composite for Absorbing-Scattering Subprocess

The RTCs just deduced are suitable for an absorbing medium. However, for an absorbing, isotropically scattering medium, part of the radiative energy represented by RTC $(V_iV_j)_{k,t-t}^{s}$, etc., is absorbed, and the rest is scattered. The following process should be carried out.

Because the following deduction implies a precondition that the energy redistributed must be unity, the RTCs for the absorbing-attenuating-reflecting subprocess should be normalized initially. That is,

$$(V_iV_j)_{k,t-t}^{s^*} = \frac{(V_iV_j)_{k,t-t}^{s}}{(4\kappa_{b,k}\Delta x_b)}, \qquad V_i \in b\text{th layer} \qquad (9a)$$

$$(V_iS_u)_{k,t-t}^{s^*} = \frac{(V_iS_u)_{k,t-t}^{s}}{(4\kappa_{b,k}\Delta x_b)}, \qquad V_i \in b\text{th layer} \qquad (9b)$$

$$(S_uV_j)_{k,t-t}^{s^*} = (S_uV_j)_{k,t-t}^{s} \qquad (9c)$$

$$(S_uS_v)_{k,t-t}^{s^*} = (S_uS_v)_{k,t-t}^{s} \qquad (9d)$$

where the asterisk denotes normalized RTCs. In fact, for improving the accuracy for calculating the scattering RTCs, we use this term,

$$\sum_{j=1}^{M_t}(V_iV_j)_{k,t-t}^{s} + (V_iS_{-\infty})_{k,t-t}^{s} + (V_iS_{+\infty})_{k,t-t}^{s}$$

instead of $4\kappa_b\Delta x_b$ to normalize $(V_iV_j)_{k,t-t}^{s}$ and $(V_iS_u)_{k,t-t}^{s}$ in Eqs. (9a) and (9b) because the value of

$$\sum_{j=1}^{M_t}(V_iV_j)_{k,t-t}^{s} + (V_iS_{-\infty})_{k,t-t}^{s} + (V_iS_{+\infty})_{k,t-t}^{s}$$

does not completely equal $4\kappa_b\Delta x_b$ due to the numerical integrating error when calculating RTC $(V_iV_j)_{k,t-t}^{s}$, etc. Take $[V_iS_u]$ to illustrate the deductive process, and, for convenience, subscripts $t-t$ and k and superscript s are omitted. Subscript a is introduced to denote the absorption quotient. Notice that only the medium scatters, not the surfaces:

1) After the first scattering event, $[V_iS_u]_a^{*1st} = (V_iS_u)^*$.

2) After the second scattering event, the energy emitted by V_i and scattered by all control volumes is

$$\sum_{l_2=1}^{M_t}\left(V_iV_{l_2}\right)^*\omega'_{l_2}$$

which can be considered equivalent to that isotropically emitted by the control volumes. This scattering event causes the portion

$$\sum_{l_2=1}^{M_t}\left(V_iV_{l_2}\right)^*\omega'_{l_2}\left(V_{l_2}S_u\right)^*$$

to be absorbed by S_u:

$$[V_iS_u]_a^{*2nd} = [V_iS_u]_a^{*1st} + \sum_{l_2=1}^{M_t}\left(V_iV_{l_2}\right)^*\omega'_{l_2}\left(V_{l_2}S_u\right)^*$$

3) Part

$$\sum_{l_2=1}^{M_t}\left(V_iV_{l_2}\right)^*\omega'_{l_2}\left[\sum_{l_3=1}^{M_t}\left(V_{l_2}V_{l_3}\right)^*\omega'_{l_3}\right]$$

of the scattered energy

$$\sum_{l_2=1}^{M_t}\left(V_iV_{l_2}\right)^*\omega'_{l_2}$$

derived in step 2 will be scattered again, and this causes some of the radiative energy, emitted by V_i, to be absorbed by S_u once more. Thus, after the third scattering event,

$$[V_i S_u]_a^{*\text{3rd}} = [V_i S_u]_a^{*\text{2nd}} + \sum_{l_2=1}^{M_t} \left(V_i V_{l_2}\right)^* \omega'_{l_2} \left[\sum_{l_3=1}^{M_t} \left(V_{l_2} V_{l_3}\right)^* \omega'_{l_3} \left(V_{l_3} S_u\right)^*\right]$$

4) The scattered energy,

$$\sum_{l_2=1}^{M_t} \left(V_i V_{l_2}\right)^* \omega'_{l_2} \left[\sum_{l_3=1}^{M_t} \left(V_{l_2} V_{l_3}\right)^* \omega'_{l_3}\right]$$

derived in step 3 will be scattered again, and this causes some of the radiative energy to be absorbed by S_u for the fourth scattering event. Thus, tracing the scattered energy repeatedly in this way until all of the control volumes satisfy the following inequality

$$\left|1 - \left\{[V_i S_{-\infty}]_a^{*\text{nth}} + \sum_{j=1}^{M_t} [V_i V_j]_a^{*\text{nth}} + [V_i S_{+\infty}]_a^{*\text{nth}}\right\}\right| < 10^{-10}$$

the calculation is finished. After the nth-order scattering event,

$$[V_i S_u]_a^{*\text{nth}} = [V_i S_u]_a^{*(n-1)\text{th}} + \sum_{l_2=1}^{M_t} \left(V_i V_{l_2}\right)^* \omega'_{l_2} \left\{\sum_{l_3=1}^{M_t} \left(V_{l_2} V_{l_3}\right)^* \omega'_{l_3} \times \left\{\sum_{l_4=1}^{M_t} \left(V_{l_3} V_{l_4}\right)^* \omega'_{l_4} \cdots \left\{\sum_{l_{n-1}=1}^{M_t} \left(V_{l_{n-2}} V_{l_{n-1}}\right)^* \omega'_{l_{n-1}} \times \left[\sum_{l_n=1}^{M_t} \left(V_{l_{n-1}} V_{l_n}\right)^* \omega'_{l_n} \left(V_{l_n} S_u\right)^*\right]\right\}\right\}\right\} \quad (10)$$

Then, $[V_i S_u]$ can be found from the inverse calculation: $[V_i S_u] = 4\alpha_b \Delta x_b [V_i S_u]_a^{*\text{nth}}$, where $V_i \in b$th layer. Similarly, after the nth scattering event, $[S_u S_v] = [S_u S_v]_a^{*\text{nth}}$, $[V_i V_j] = 4\alpha_b \Delta x_b [V_i V_j]_a^{*\text{nth}}$, and $[S_u V_j] = [S_u V_j]_a^{*\text{nth}}$ can be determined, where

$$[S_u S_v]_a^{*\text{nth}} = [S_u S_v]_a^{*(n-1)\text{th}} + \sum_{l_2=1}^{M_t} \left(S_u V_{l_2}\right)^* \omega'_{l_2} \left\{\sum_{l_3=1}^{M_t} \left(V_{l_2} V_{l_3}\right)^* \omega'_{l_3} \times \left\{\sum_{l_4=1}^{M_t} \left(V_{l_3} V_{l_4}\right)^* \omega'_{l_4} \cdots \left\{\sum_{l_{n-1}=1}^{M_t} \left(V_{l_{n-2}} V_{l_{n-1}}\right)^* \omega'_{l_{n-1}} \times \left[\sum_{l_n=1}^{M_t} \left(V_{l_{n-1}} V_{l_n}\right)^* \omega'_{l_n} \left(V_{l_n} S_v\right)^*\right]\right\}\right\}\right\} \quad (11)$$

$$[V_i V_j]_a^{*\text{nth}} = [V_i V_j]_a^{*(n-1)\text{th}} + \sum_{l_2=1}^{M_t} \left(V_i V_{l_2}\right)^* \omega'_{l_2} \left\{\sum_{l_3=1}^{M_t} \left(V_{l_2} V_{l_3}\right)^* \omega'_{l_3} \times \left\{\sum_{l_4=1}^{M_t} \left(V_{l_3} V_{l_4}\right)^* \omega'_{l_4} \cdots \left\{\sum_{l_{n-1}=1}^{M_t} \left(V_{l_{n-2}} V_{l_{n-1}}\right)^* \omega'_{l_{n-1}} \times \left[\sum_{l_n=1}^{M_t} \left(V_{l_{n-1}} V_{l_n}\right)^* \omega'_{l_n} \left(V_{l_n} V_j\right)^* \eta_j\right]\right\}\right\}\right\} \quad (12)$$

$$[S_u V_j]_a^{*\text{nth}} = [S_u V_j]_a^{*(n-1)\text{th}} + \sum_{l_2=1}^{M_t} \left(S_u V_{l_2}\right)^* \omega'_{l_2} \left\{\sum_{l_3=1}^{M_t} \left(V_{l_2} V_{l_3}\right)^* \omega'_{l_3} \times \left\{\sum_{l_4=1}^{M_t} \left(V_{l_3} V_{l_4}\right)^* \omega'_{l_4} \cdots \left\{\sum_{l_{n-1}=1}^{M_t} \left(V_{l_{n-2}} V_{l_{n-1}}\right)^* \omega'_{l_{n-1}} \times \left[\sum_{l_n=1}^{M_t} \left(V_{l_{n-1}} V_{l_n}\right)^* \omega'_{l_n} \left(V_{l_n} V_j\right)^* \eta_j\right]\right\}\right\}\right\} \quad (13)$$

Validations of Physical Model and Calculation Procedure

Validations of RTCs

The correctness of the spectral RTCs is first validated by Eq. (4) and the following equation:

$$\sum_{j=1}^{M_t} [V_i V_j]_{k,t-t}^s + [V_i S_{-\infty}]_{k,t-t}^s + [V_i S_{+\infty}]_{k,t-t}^s = 4\alpha_b \Delta x_b \quad V_i \in b\text{th layer} \quad (14a)$$

$$[S_{-\infty} S_{-\infty}]_{k,t-t}^s + \sum_{j=1}^{M_t} [S_{-\infty} V_j]_{k,t-t}^s + [S_{-\infty} S_{+\infty}]_{k,t-t}^s = 1 \quad (14b)$$

$$[S_{+\infty} S_{-\infty}]_{k,t-t}^s + \sum_{j=1}^{M_t} [S_{+\infty} V_j]_{k,t-t}^s + [S_{+\infty} S_{-\infty}]_{k,t-t}^s = 1 \quad (14c)$$

The RTC expression (8) is numerically calculated by a 30-point improved Gaussian quadrature scheme. The precision of Gaussian quadrature scheme is chosen as 10^{-9}, and, with this precision, the errors for the satisfaction of Eqs. (4) and (14) are smaller than 10^{-10}. Hence, Eqs. (4) and (14) are satisfied very well. (Please refer to Ref. 20 to get more information about how the satisfaction of Eqs. (4) and (14) is checked.)

Comparison with Refs. 12 and 22

Reference 12 investigated the radiative heat transfer in an isothermal layer with specular semitransparent boundaries. Hence, comparison with the current results helps to validate the specular model of this paper. Figure 4 shows the comparison. The

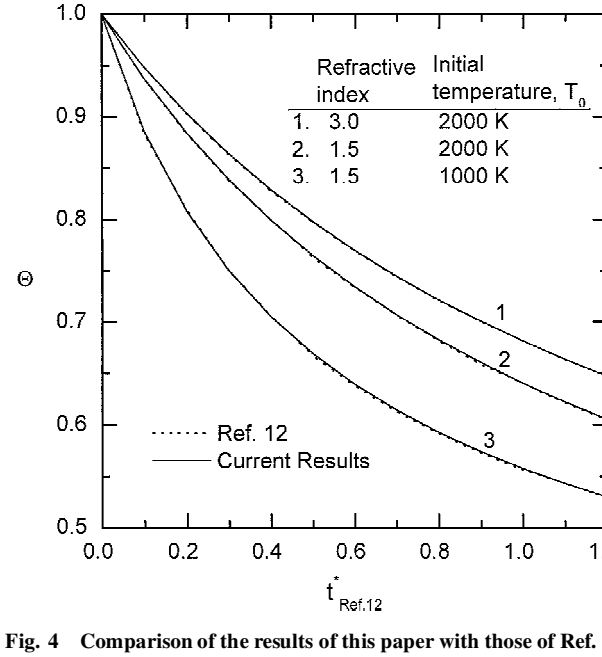

Fig. 4 Comparison of the results of this paper with those of Ref. 12.

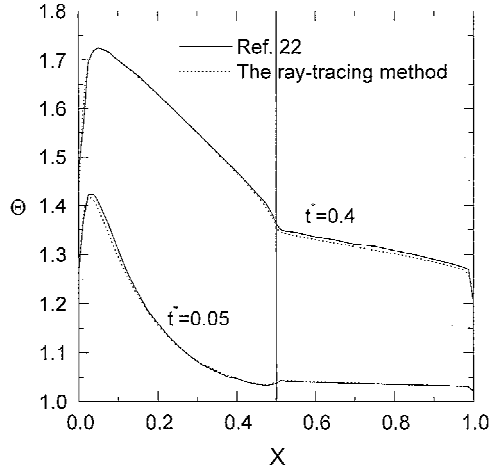

Fig. 5 Comparison of the results of the multilayer diffuse reflection model of the ray-tracing method with those of Ref. 22.

dotted curves are the results of Ref. 12 by the use of the following parameters: $\alpha_k = 20$, 400, and 10,000 m^{-1} corresponding to $\lambda = 0 \sim 2.7$, $2.7 \sim 4.4$, and $4.4 \sim \infty$ μm, respectively, $L_1 = 0.005$ m, $T_{-\infty} = T_{+\infty} = 300$ K, and $T_r = T_0$. The initial temperature and the refractive indexes are indicated in Fig. 4. The dimensionless time is defined by Ref. 12 as $t^*_{\text{Ref. 12}} = \sigma T_r^3 t/(\rho_1 c_1 L_t)$. Let the layer number $n = 1$, then, take the whole layer as one control volume ($M_t = M_1 = 1$), and choose the conduction–radiation parameter as very small, $N_1 = 10^{-100}$. Then, the multilayer specular model of this paper can also calculate isothermal layer results for pure radiation. As shown in Fig. 4, the current results agree well with those of Ref. 12.

Siegel[22] investigated transient coupled heat transfer in a two-layer composite with spectral properties. The surfaces and the interface of the two-layer composite are semitransparent and diffuse. The ray-tracing method also can be used to investigate the transient coupled radiative and conductive heat transfer in a multilayer composite with semitransparent and diffuse interfaces, and so the results of the multilayer diffuse reflection model of the ray-tracing method can be compared with those of Ref. 22. The comparison with Ref. 22 can validate the correctness of the discrete boundary condition of this paper, Eq. (3), which is the same as that for the multilayer diffuse reflection model of the ray-tracing method. The calculating parameters are $n = 2$, $T_{-\infty} = 2T_r$, $T_{+\infty} = T_0 = T_{g1} = T_{g2} = T_r$, $\rho_1 c_1 = \rho_2 c_2$, $h_1/(\sigma T_r^3) = h_2/(\sigma T_r^3) = 4$, $L_1 = L_2$, $n_1 = 1.5$, $n_2 = 3$, and $N_1 = N_2 = 0.015$. The optical properties of the two-layer composite is expressed by two spectral bands with cutoff $\lambda T_r = 4000$ μmK: $\omega_{1,1} = 0.7101$, $\omega_{1,2} = 0.98$, $\tau_{1,1} = 6.9$, $\tau_{1,2} = 5$, $\omega_{2,1} = \omega_{2,2} = 0$, $\tau_{2,1} = 5$, and $\tau_{2,2} = 0.5$. As shown in Fig. 5, good agreement is obtained. This proves that the discrete boundary condition (3), the spectral band model, the numerical method, the multilayer ray-tracing method, and the isotropic scattering theory of this paper are correct.

In addition, the numerical methods used herein are the same as those used in Ref. 20. (Please refer to Ref. 20 for more information about the numerical methods.)

Results and Discussions

As shown in Eq. (1), transient coupled heat transfer in a multilayer composite with spectral properties can be studied. The comparison of the results of this paper with those of Ref. 12 in Fig. 4, and the comparison of the results of the multilayer diffuse reflection model of the ray-tracing method with those of Ref. 22 in Fig. 5, wherein the effects of spectral properties of medium on radiative heat transfer have been investigated, proves that the spectral band model of this paper is correct. However, for simplicity, only transient heat transfer in a gray multilayer composite is investigated in this section. The node number of each layer M_b is chosen until the total steady-state heat flux and the steady-state temperature at each node almost reach

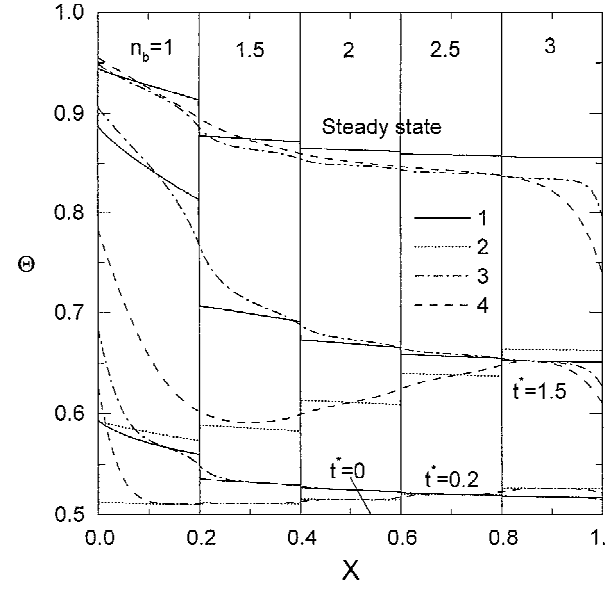

a) $\kappa_b = 50$ m^{-1}

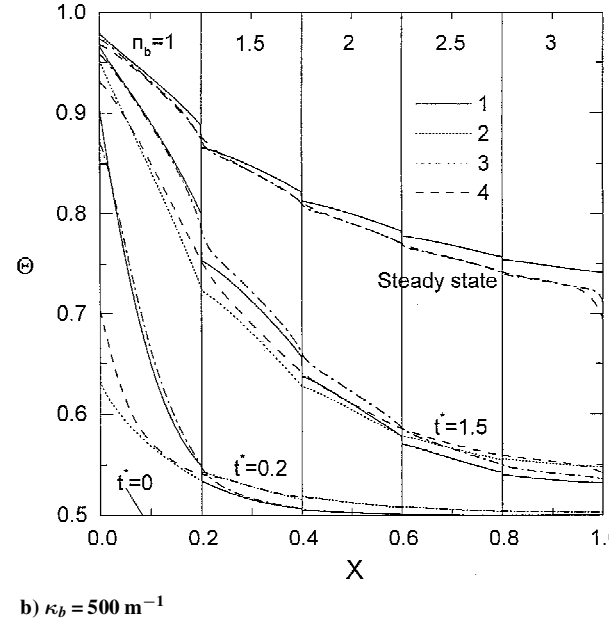

b) $\kappa_b = 500$ m^{-1}

Fig. 6 Temperature profile for refractive indexes arranged in increasing order along the thickness of the composite slab.

constant values.[19] From Figs. 6–8, the number of control volumes is chosen as $M_b = 100$ ($b = 1$–n). $M_b = 25$ is chosen for Fig. 9. A constant time step, $\Delta t^* = t^*/300$, is applied, and the steady state is said to be reached if $\max |T_i^{m+1} - T_i^m| < 10^{-5}$.

These parameters are constants in the following calculations: $\rho_b c_b = \text{constant}$ ($b = 1$–n), $T_0 = 500$ K, $T_r = 1000$ K, $T_{-\infty} = T_{g1} = 1000$ K, and $T_{+\infty} = T_{g2} = 500$ K. The following stipulations are specified for Figs. 6–9:

1) Curve 1 ($\omega_b = 0$, where $b = 1$–n) and curve 2 ($\omega_b = 0.9$) are for pure radiation. For this condition, the conduction–radiation parameter of each layer is assigned to be very small in the calculation, such as $N_b = 10^{-100}$ ($b = 1$–n), and $h_1 = h_2 = 0$ Wm^{-2} K^{-1}. Hence, there is no conduction within the composite, and the composite does not exchange convective energy with the surrounding fluids.

2) Curve 3 ($\omega_b = 0$) and curve 4 ($\omega_b = 0.9$) are for coupled heat transfer in the composite with $N_b = 0.006$ and $h_1 = h_2 = 10$ Wm^{-2} K^{-1}. For these cases, in addition to exchanging radiative energy with the surrounding black surfaces, the composite exchanges convective energy with the surrounding fluids as well, and there is interaction of conduction and radiation within the composite.

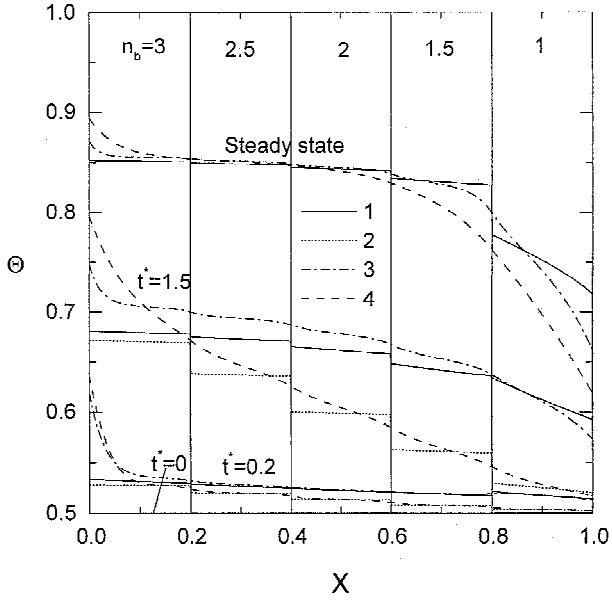

a) $\kappa_b = 50\ \mathrm{m}^{-1}$

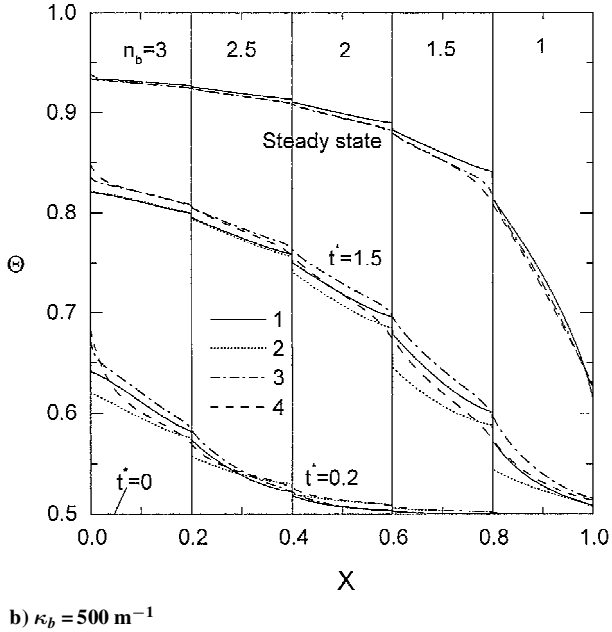

b) $\kappa_b = 500\ \mathrm{m}^{-1}$

Fig. 7 Temperature profile for refractive indexes arranged in decreasing order along the thickness of the composite slab.

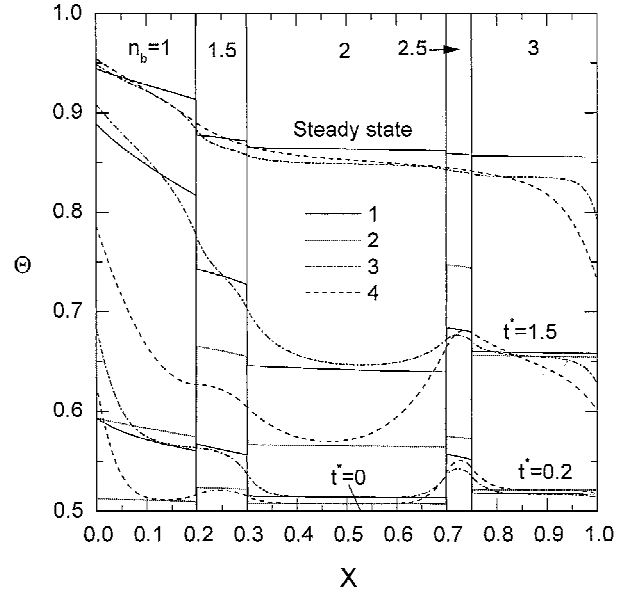

a) Refractive indexes arranged in increasing order along the thickness of the composite slab

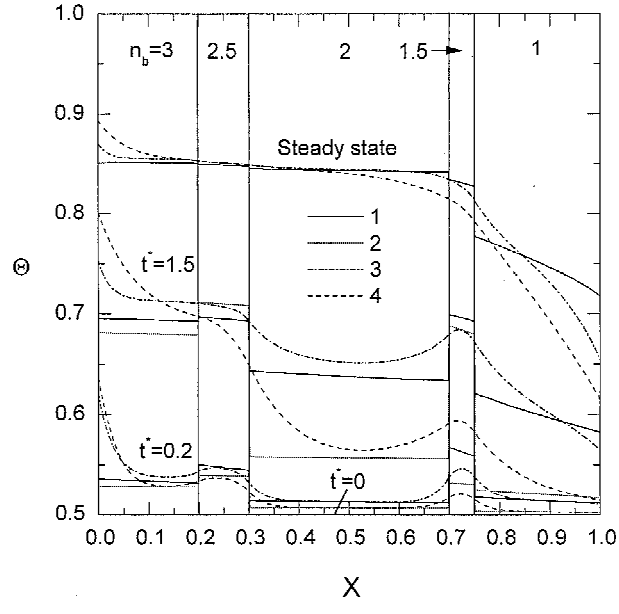

b) Refractive indexes arranged in decreasing order along the thickness of the composite slab

Fig. 8 Effect of layer thickness on heat transfer.

Effect of Refractive Index Arrangement on Heat Transfer

The effect on heat transfer of the refractive indexes being arranged in increasing order along the thickness of a five-layer composite is shown in Fig. 6a ($\kappa_b = 50\ \mathrm{m}^{-1}$, where $b = 1$–n) and Fig. 6b ($\kappa_b = 500\ \mathrm{m}^{-1}$), where the thickness of each layer of the composite is the same, $L_b = 0.004$ m ($b = 1$–n).

As shown in Fig. 6a, for pure radiation (curves 1 and 2), there is a discontinuity in the temperature at both sides of each interface. When there is no scattering (curve 1), the average temperature of each layer decreases along the whole thickness. Because there is no reflection at surface S_1 (because $n_1 = 1$), all of the radiative energy emitted by $S_{-\infty}$ enters the first layer. On the other hand, there is reflection occurring at the interface between the first layer and the second layer, so that the first layer absorbs most of the radiative energy, and the radiative energy entering the following layers decreases. These conditions cause the first layer to have the highest temperature and the temperature difference at the interface between the first layer and the second layer to be largest.

However, different results occur for the addition of isotropic scattering. As shown by curve 2, for a short time the highest temperature appears in the fifth layer, the lowest temperature appears in the first layer, and the average temperature of each layer increases along the whole thickness. This shows that the introduction of scattering causes the layer with the bigger refractive index to absorb more radiative energy. This phenomenon is mainly caused by total reflection. As shown in Fig. 6, total reflection will occur at the right side of every interface of the composite. When the radiative energy emitted by $S_{-\infty}$ enters the composite from S_1, the media of the composite absorbs little, and most of it is scattered. If the incident angle of the scattered energy is greater than the critical angle of an interface, total reflection occurs at the right side of the interface, and this inhibits scattered radiative energy transferring from right to left. Hence, the larger the refractive indexes of the interfaces that are located on the left of a layer, the more the scattered energy is reflected back, and the higher the temperature of the layer is. As the process gradually evolves, the temperatures of all layers increase, and, at steady state, curve 2 superposes with curve 1 completely. The dimensionless steady heat fluxes of the two curves are also the same

Table 1 Dimensionless steady heat flux ($\tilde{q}^t$)

	Fig. 6		Fig. 7		Fig. 8		Fig. 9	
Curve	a	b	a	b	a	b	a	b
1	0.4531	0.1821	0.4531	0.1821	0.4531	0.4531	0.2911	0.2911
2	0.4531	0.1821	0.4531	0.1821	0.4531	0.4531	0.2911	0.2911
3	0.4840	0.1993	0.4748	0.1977	0.4840	0.4747	0.3086	0.3063
4	0.4779	0.1975	0.4709	0.1964	0.4774	0.4709	0.3043	0.3023

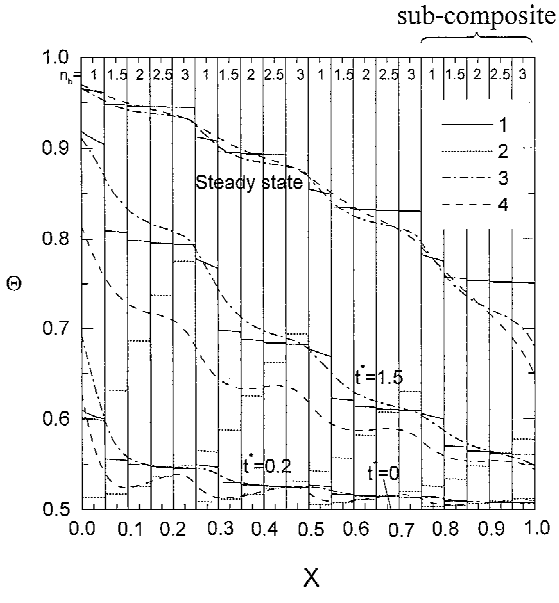

a) Refractive indexes arranged in increasing order along the thickness of each subcomposite

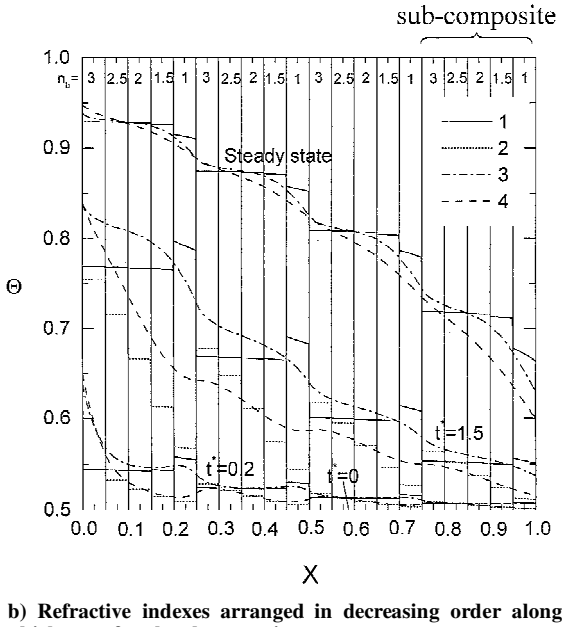

b) Refractive indexes arranged in decreasing order along the thickness of each subcomposite

Fig. 9 Effect of layer number and refractive index arrangement on heat transfer ($\kappa_b = 50$ m^{-1}).

(Table 1). This is a well-known conclusion that isotropic scattering exerts no influence on radiative equilibrium.

As for coupled heat transfer (curves 3 and 4), the heating of the left side fluid causes the temperature of S_1 to increase. The cooling of the right side's low-temperature fluid causes the temperature of S_2 to decrease. The dimensionless steady heat fluxes are bigger than those of pure radiation, and the discontinuity of temperature at all interfaces disappears. Curves 3 and 4 almost cross curves 1 and 2, respectively, for a short time. This clearly shows how conduction affects the pure radiation temperature distribution of the composite. When the media scatters isotropically, as shown by curve 4, a minimum temperature appears within the composite for a short time, and the dimensionless steady heat flux is somewhat smaller than that without scattering (curve 3).

As shown in Fig. 6b, when the extinction coefficient of each layer increases ($\kappa_b = 500$ m^{-1}), the radiative energy emitted by $S_{-\infty}$ is strongly absorbed by the medium close to the surface of the first layer, and so the temperature of S_1 and the medium close to the surface rises quickly, especially as shown by curves 1 and 3. The temperature gradient in each layer increases, and the dimensionless steady heat flux decreases greatly (Table 1). Because of the large extinction coefficient of each layer, as shown by curve 2, initially, isotropic scattering can not cause the average temperatures of the layers to increase along the whole thickness of the composite as compared to the same case for a smaller extinction coefficient (Fig. 6a). In addition, no minimum temperature appears for the cases of coupled heat transfer with scattering (curve 4) in Fig. 6b, as compared to Fig. 6a. At steady state, curves 2 and 1 are superposed on each other, and isotropic scattering decreases the steady heat flux of coupled heat transfer as well.

The effect on heat transfer of arranging the refractive indexes in decreasing order along the slab thickness are shown in Figs. 7a and 7b. Except for refractive index, the other parameters of Figs. 7a and 7b are the same as those of Figs. 6a and 6b. Compared with Figs. 6a and 6b, we can see that radiation causes the steady-state temperature curves to concave downward. The dimensionless steady heat fluxes for the cases of pure radiation (curves 1 and 2) in Figs. 7a and 7b are equal to those for the same cases (curves 1 and 2) in Figs. 6a and 6b, so that reversing the refractive index values has no influence on steady-state heat flux for radiative equilibrium. This conclusion is the same as that of Ref. 2. The reason is that, on one hand, when the refractive index of one layer increases, the ability of the media of the layer to emit radiative energy is intensified, and this causes the steady-state flux to increase. On the other hand, the reflection and total reflection at the interfaces of the composite are also intensified, and this decreases steady-state heat flux because the intensified reflection prevents radiative energy propagation from left to right. However, for pure radiative heat transfer conditions, when the refractive index arrangement of the composite is reversed, these two effects on increasing and decreasing steady-state heat flux compensate for each other and keep the steady-state heat flux unchanged. However, for coupled heat transfer conditions, the steady heat fluxes (curves 3 and 4) in Figs. 6a and 6b are smaller than those of coupled heat transfer (curves 3 and 4) in Figs. 6a and 6b (Table 1). Arranging the refractive indexes such that they increase along the slab's thickness is advantageous for coupled heat transfer. This can be explained from Figs. 6a and 7a. As shown in Fig. 6a, for pure radiation and steady-state conditions (curves 1 and 2), the temperature gradients in the first layer are much larger than those in the other four layers, and the temperature curve concaves upward. These features, caused by radiation, are advantageous for convective heating on the left surface when conductive heat transfer is added to the composite because of the large temperature gradient in the medium near surface S_1. However, it is disadvantageous for convective cooling on the right surface due to the small temperature gradient in the medium near surface S_2, but in Fig. 7a, the contrary condition occurs. That is, the effect of radiation on temperature distribution is advantageous for convective cooling on the right surface and disadvantageous for convective heating on the left surface when conductive heat transfer

is considered. By comparison of the results shown in Fig. 7a (for which the right surface is cooled by the intensified convective) to the results shown in Fig. 6a (for which the left surface is heated by intensified convective), heat flux can be increased considerably. What should be pointed out is that if there is no convective heat transfer on both surfaces when conductive heat transfer is added to the composite, the coupled steady-state heat flux for the case of the refractive index arrangement in Fig. 7a is larger than that for the case of the refractive index arrangement in Fig. 6a.

As shown by curve 2 in Fig. 7a, the average transient temperature of each layer decreases along the slab's thickness when scattering is added. For coupled heat transfer, comparing curve 4 with curve 3, we can see that scattering can make the temperatures of surface S_1 and the media near the surface increase. This trend can be understood because the smaller absorption coefficient of each layer, which is produced by adding scattering, causes a decrease in the ability of each layer to emit energy. Then the convective energy, received from the left surrounding fluid at a high temperature, can not be reemitted adequately by the media near surface S_1 due to the smaller absorption coefficient therein, and so it accumulates within the layer. The steady heat flux for scattering cases (curve 4) is smaller than that for nonscattering cases (curve 3) due to the resistance caused by scattering (Table 1).

The large extinction coefficient of Fig. 7b weakens the effect of radiative transfer between two distant nodes. Compared with Fig. 7a, the curves in Fig. 7b get closer, the temperature gradient increases, and the steady-state heat flux greatly decreases.

Effect of Layer Thickness on Heat Transfer

Let the optical thickness ($\tau_b = \kappa_b L_b = 0.2$, where $b = 1$–n) and other parameters of each layer in Fig. 6a and Fig. 7a remain unchanged. Then change the thickness of each layer to $L_1 = 0.004$, $L_2 = 0.002$, $L_3 = 0.008$, $L_4 = 0.001$, and $L_5 = 0.005$ m. The results are shown in Figs. 8a and 8b. As shown by the cases for radiation only (curves 1 and 2), the temperatures of the second and the fourth layers are higher than those of other layers at shorter times due to their large extinction coefficients. The two curves are still superposed on each other at steady state and have equal steady heat fluxes, which are the same as those of comparable cases in Figs. 6a and 7a. For a short time, two maximum temperatures appear in the second and the fourth layers when conduction and convection are included (curves 3 and 4), and two minimum temperatures appear in the first and the third layers. The steady heat fluxes for cases including conduction and convection (curves 3 and 4) are almost the same as those of the corresponding cases (curves 3 and 4) in Figs. 6a and 7a.

Effect of Layer Number and Arrangement of Refractive Index on Heat Transfer

For this case, each layer of Fig. 6a was divided into four equal parts, and the resulting 20 layers were rearranged as shown in Figs. 9a and 9b to compose a new 20-layer composite, which can be considered a combination of four similar subcomposites, each of which contained five layers. In Fig. 9a, the refractive index arrangement in each subcomposite is from small to large along the direction of increasing thickness, but reversed in Fig. 9b. As shown in Figs. 9a and 9b, the temperature distribution shows some complex periodicity.

As shown for radiation only (curves 1 and 2) in Fig. 9a, the temperature distribution in each subcomposite is similar to that shown for the same cases in Fig. 6a. The average temperature of each subcomposite decreases along the slab's thickness, and the two curves are superposed on each other at steady state. Just as the temperature distribution for pure radiation shows some periodicity, the temperature distributions for coupled heat transfer also are periodic, as shown by curves 3 and 4. The steady-state heat fluxes of coupled heat transfer are larger than those for pure radiation because the transfer energy is increased by combining conduction and convection. The steady heat flux for the scattering case (curve 4) is smaller than that for the nonscattering case (curve 3), and curve 4 is smoother than curve 3 at steady state because the scattering of a medium can distribute radiative energy more uniformly within a layer. A comparison with Fig. 6a shows that, though the total optical thickness of the composite does not change, the steady heat fluxes are greatly reduced (Table 1) because the stronger reflection, caused by the increased refractive indexes at interfaces within the composite, resists the radiative energy transferring from left to right.

The same type of periodicity is shown in Fig. 9b. As shown by curve 1, for the pure radiation case, the temperature distribution in each subcomposite is similar to that for the same case in Fig. 7a at steady state, but the temperature of the fifth layer of each subcomposite is obviously higher than that of other layers of the same subcomposite. The main reason for this is that, the radiative energy, absorbed by the fifth layer of each subcomposite from $S_{-\infty}$ or other layers, can not be reemitted adequately because of its unit refractive index. In Fig. 7a, the fifth layer can be cooled better because it directly faces $S_{+\infty}$, which has a low temperature. This phenomenon is shown to some degree by curve 1 at $t^* = 0.2$. The steady-state heat fluxes for coupled heat transfer (curves 3 and 4) in Fig. 8b are smaller than those in Fig. 8a. The reasons are the same as the explanations for Figs. 6 and 7. From the preceding analysis, we can see that the heat transfer periodicity in Figs. 8a and 8b is similar to that in Figs. 6a and 7a.

Conclusions

Transient coupled radiative and conductive heat transfer in a multilayer absorbing, isotropically scattering composite with semitransparent and specular surfaces and interfaces has been investigated. The specular reflectivities of all surfaces and interfaces are determined by Fresnel's reflective law and Snell's refractive law. By the creation of one-layer and multilayer radiative intensity transfer functions, the transfer process of radiative intensity in the multilayer composite can be easily traced, and an attenuation expression can be obtained. When the whole hemispherical space is integrated over to solve for the RTCs, the complex total reflection problem of the multilayer composite can be solved by the following two steps: 1) dividing the interval of integration for the whole hemispherical space into many intervals that are separated by critical angles arranged from small to large (or from large to small) and 2) using Snell's refractive law to determine the reflection occurring at the interfaces and surfaces. The RTCs of the multilayer composite are used to calculate the radiative source term in the overall conservation of energy equation,[16] and that energy equation is solved by the universal fully implicit discrete control-volume method.

Comparing our results with those of Ref. 12 for a single layer has helped to validate the RTCs computed from Eqs. (4) and (14). This provides confidence in our solutions. The effects of refractive indexes on pure radiative and coupled heat transfer are investigated simultaneously. The analysis of our results shows the following:

1) When the extinction coefficient of each layer constant is kept, adding isotropic scattering decreases the coupled steady-state heat flux, as compared to the condition with no scattering.

2) For the case of a composite with hot surroundings (heating the composite by radiation and convection simultaneously) on one side and cold surroundings (cooling the composite by radiation and convection simultaneously) on the other side, the coupled steady-state heat flux for increasing the refractive index from the hot to the cold side is greater than that found for a decreasing refractive index.

3) If the refractive index varies periodically through the layers of a composite slab, and all other parameters in each layer are the same, the temperature distribution throughout the composite has a periodic variation superimposed on the overall results that are found without a periodic refractive index.

4) As the number of layers and interfaces increase, but the total thickness and the total optical thickness of the composite are kept unchanged, reflection is strengthened, and so the steady heat flux decreases.

Appendix A: Determination of Reflectivity

The radiative intensity emitted by the mth element at angle θ will enter the bth layer from P_{b-1} or P_b, which are the two boundaries of

the bth layer. Then it will be reflected many times within this layer at angle θ_b, which is the refractive angle in the bth layer. According to Snell's refractive law, it can be expressed as

$$\theta_b = \arcsin(\sin\theta n_m / n_b) \tag{A1}$$

where n_m is the refractive index of the mth element.

When the radiative intensity propagates from the bth layer to its neighboring oth ($o = b-1$ or $b+1$) layer at angle θ_b, the reflectivity at the interface $\rho(\theta_b)_{bo}$ is function of the polarized components. For a perfect dielectric ideal medium, the effect of the extinction coefficient in the complex index of refraction can be neglected. According to electromagnetic theory, if total reflection does not occur, then[12,23]

$$\rho_{//}(\theta_b)_{bo} = \left[\frac{\tan(\theta_b - \varphi_o)}{\tan(\theta_b + \varphi_o)}\right]^2 \tag{A2a}$$

for a parallel component

$$\rho_{\perp}(\theta_b)_{bo} = \left[\frac{\sin(\theta_b - \varphi_o)}{\sin(\theta_b + \varphi_o)}\right]^2 \tag{A2b}$$

for a perpendicular component, where φ_o is refractive angle of the oth layer, and[23]

$$\varphi_o = \arcsin(n_b / n_o \sin\theta_b) \tag{A3}$$

When $n_b > n_o$, and $\theta_b > \arcsin(n_o/n_b)$, then total reflection occurs, that is, $\rho(\theta_b)_{bo} = 1$. If $n_b = n_o$, then $\rho(\theta_b)_{bo} = 0$.

By the substitution of Eq. (A1) into Eqs. (A2) and (A3), the reflectivity $\rho(\theta_b)_{bo}$ can be written as $\rho(\theta)_{bo}$, which is only a function of θ. By the substitution of Eq. (A1) into the preceding inequality, $\theta_b > \arcsin(n_o/n_b)$. Whether or not total reflection occurs at the interface can be determined by the angle θ. Hence, when any element (surface or control volume) emits radiative intensity at angle θ, the reflectivity of all of the interfaces and the total reflections occurring therein are determined by the angle θ.

Conversely, if a ray propagates from the oth layer to the bth layer at an incident angle φ_o, θ_b becomes the refractive angle. Then, as shown in Eq. (A2), $\rho(\varphi_o)_{ob} = \rho(\theta_b)_{bo}$.

Appendix B: Single-Layer Semitransparent Medium Radiative Intensity Transfer Model

For the specular reflection condition, we can trace a ray (emitted at a specific angle) along its journey to obtain an attenuation expression. The equations that describe radiative intensity propagation in a single layer are defined as single-layer radiative intensity transfer functions, expressed by the symbol $\boldsymbol{F}^{a2_b}_{a1_b,k}$, which is the ratio of the spectral radiative intensity received by control volume or interface $a2_b$ to that emitted by control volume or interface $a1_b$ in the kth spectral band. Whether the medium is gray or nongray, the formulation and the deductive processes are the same; and so subscript k is omitted here.

As shown in Fig. B1 assume $P_{b-1'}$ or P_b emits radiative intensity at angle θ_b. Then it will be reflected and attenuated many times within this layer until it becomes zero. When this process is traced, the following radiative intensity quotient functions are obtained[19,20]:

$$\boldsymbol{F}^{V_{I_b}}_{P_{b-1'}} = \left\{\rho(\theta_b)_{b,b+1}\exp\left[-\kappa_b\left(L_b + x^{P_b}_{(I+1)_b}\right)/\mu_b\right] + \exp\left(-\kappa_b x^{P_{b-1'}}_{I_b}/\mu_b\right)\right\}[1-\exp(-\kappa_b\Delta x_b/\mu_b)]/(1-\beta_1)$$

$$\boldsymbol{F}^{V_{I_b}}_{P_b} = \left\{\rho(\theta_b)_{b,b-1}\exp\left[-\kappa_b\left(L_b + x^{P_{b-1'}}_{I_b}\right)/\mu_b\right] + \exp\left(-\kappa_b x^{P_b}_{(I+1)_b}/\mu_b\right)\right\}[1-\exp(-\kappa_b\Delta x_b/\mu_b)]/(1-\beta_1)$$

$$\boldsymbol{F}^{P_b}_{P_b} = \exp(-2\kappa_b L_b/\mu_b)\rho(\theta_b)_{b,b-1}/(1-\beta_1),$$

$$\boldsymbol{F}^{P_{b-1'}}_{P_{b-1'}} = \exp(-2\kappa_b L_b/\mu_b)\rho(\theta_b)_{b,b+1}/(1-\beta_1)$$

$$\boldsymbol{F}^{P_b}_{P_{b-1'}} = \boldsymbol{F}^{P_{b-1'}}_{P_b} = \exp(-\kappa_b L_b/\mu_b)/(1-\beta_1) \tag{B1a}$$

where $x^{P_b}_{(I+1)_b} = L_b - I_b\Delta x_b$, $x^{P_{b-1'}}_{I_b} = (I_b - 1)\Delta x_b$, $\beta_1 = \exp(-2\kappa_b L_b/\mu_b)\rho(\theta_b)_{b,b-1}\rho(\theta_b)_{b,b+1} < 1$, $\mu_b = \cos\theta_b$, and θ_b is the incident angle.

The radiative intensity emitted by V_{I_b} is also reflected and attenuated many times within this layer until it becomes zero. When this process is traced, the other radiative intensity quotient transfer functions can be obtained[19,20]:

$$\boldsymbol{F}^{P_b}_{V_{I_b}} = \boldsymbol{F}^{V_{I_b}}_{P_b}, \qquad \boldsymbol{F}^{P_{b-1'}}_{V_{I_b}} = \boldsymbol{F}^{V_{I_b}}_{P_{b-1'}}$$

$$\boldsymbol{F}^{V_{J_b}}_{V_{I_b}} = \left\{\exp\left(-\kappa_b x^{J_b}_{I_b}/\mu_b\right) + \rho(\theta_b)_{b,b-1}\exp\left[-\kappa_b\left(x^{P_{b-1'}}_{I_b} + x^{P_{b-1'}}_{J_b}\right)/\mu_b\right] + \rho(\theta_b)_{b,b+1}\exp\left[-\kappa_b\left(x^{P_b}_{(I+1)_b} + x^{P_b}_{(J+1)_b}\right)/\mu_b\right] + \rho(\theta_b)_{b,b-1}\rho(\theta_b)_{b,b+1}\exp\left[-\kappa_b\left(2L_b - 2\Delta x_b - x^{J_b}_{I_b}\right)/\mu_b\right]\right\} \times [1-\exp(-\kappa_b\Delta x_b/\mu_b)]^2/(1-\beta_1)$$

$$\boldsymbol{F}^{V_{I_b}}_{V_{I_b}} = \left\{\rho(\theta_b)_{b,b-1}\exp\left(-2\kappa_b x^{P_{b-1'}}_{I_b}/\mu_b\right) + \rho(\theta_b)_{b,b+1}\exp\left(-2\kappa_b x^{P_b}_{(I+1)_b}/\mu_b\right) + 2\rho(\theta_b)_{b,b-1}\rho(\theta_b)_{b,b+1} \times \exp\left[-\kappa_b\left(x^{P_{b-1'}}_{I_b} + L_b + x^{P_b}_{(I+1)_b}\right)/\mu_b\right]\right\} \times [1-\exp(-\kappa_b\Delta x_b/\mu_b)]^2/(1-\beta_1) \tag{B1b}$$

where $x^{J_b}_{I_b}$ is the distance between V_{I_b} and V_{J_b}, as shown in Fig. B1, and $x^{J_b}_{I_b} = (|I-J|-1)\Delta x_b$.

The preceding equation for $\boldsymbol{F}^{V_{I_b}}_{V_{I_b}}$ represents the quotient of the radiative intensity received by V_{I_b} (superscript) to that emitted by V_{I_b} (subscript), traversing between the two boundaries I_b and $(I+1)_b$ of V_{I_b}, and transferring within the layer until it reduces to zero. However, before the radiative energy emitted by V_{I_b} over the whole space traverses the two boundaries I_b and $(I+1)_b$, part of it is absorbed by V_{I_b} itself, and this is considered as

$$4\kappa_b\Delta x_b - 2\left\{1 - 2\int_0^1 \mu\exp\left[-\frac{(\kappa_b\Delta x_b)}{\mu}\right]\mathrm{d}\mu\right\}$$

that is, this term must be added when calculating $(V_{I_b}V_{I_b})^s_{t-t}$.

The reflectivities, $\rho(\theta_b)_{b,b-1}$ and $\rho(\theta_b)_{b,b+1}$, in Eqs. (B1) are determined as discussed in Appendix A. Thus, corresponding to the two parallel and perpendicular components, there are different values for Eqs. (B1). In addition, for the first and the nth layer, P_0 and P_n appear in Eqs. (B1), and they should be replaced by S_1 and S_2, respectively.

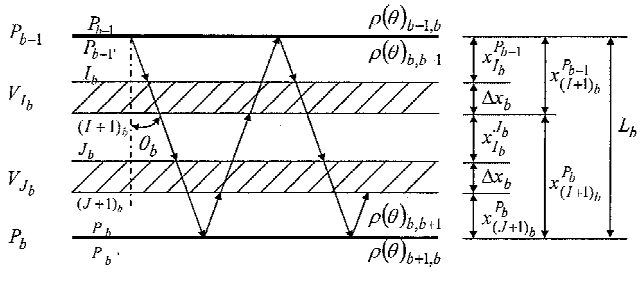

Fig. B1 Single-layer semitransparent medium radiative intensity transfer model.

Acknowledgments

This research is supported by the Chinese National Science Fund for Distinguished Young Scholars (59725617) and by the Doctorial Subject Special Fund of the High School of the Ministry of Education of China.

References

[1]Siegel, R., and Spuckler, C. M., "Refractive Index Effects on Radiation in an Absorbing, Emitting, and Scattering Laminated Layer," *Journal of Heat Transfer*, Vol. 115, No. 1, 1993, pp. 194–200.

[2]Siegel, R., and Spuckler, C. M., "Variable Refractive Index Effects on Radiation in Semitransparent Scattering Multilayered Regions," *Journal of Thermophysics and Heat Transfer*, Vol. 7, No. 4, 1993, pp. 624–630.

[3]Spuckler, C. M., and Siegel, R., "Refractive Index Effects on Radiative Behavior of a Heated Absorbing-Emitting Layer," *Journal of Thermophysics and Heat Transfer*, Vol. 6, No. 4, 1992, pp. 596–604.

[4]Siegel, R., "Refractive Index Effects on Transient Cooling of a Semitransparent Radiating Layer," *Journal of Thermophysics and Heat Transfer*, Vol. 9, No. 1, 1995, pp. 55–62.

[5]Siegel, R., "Transient Thermal Analysis of Parallel Translucent Layers by Using Green's Functions," *Journal of Thermophysics and Heat Transfer*, Vol. 13, No. 1, 1999, pp. 10–17.

[6]Liu, C. C., and Dougherty, R. L., "Anisotropically Scattering Media Having a Reflective Upper Boundary," *Journal of Thermophysics and Heat Transfer*, Vol. 13, No. 2, 1999, pp. 177–184.

[7]Crosbie, A. L., and Shieh, S. M., "Three-Dimensional Radiative Transfer for Anisotropic Scattering Medium with Refractive Index Greater Than Unity," *Journal of Quantitative Spectroscopy and Radiative Transfer*, Vol. 44, No. 2, 1990, pp. 299–312.

[8]Schwander, D., Flamant, G., and Olalde, G., "Effects of Boundary Properties on Transient Temperature Distributions in Condensed Semitransparent Media," *International Journal of Heat and Mass Transfer*, Vol. 41, No. 14, 1998, pp. 2083–2096.

[9]Tan, H. P., and Lallemand, M., "Transient Radiative-Conductive Heat Transfer in Flat Glasses Submitted to Temperature, Flux and Mixed Boundary Conductions," *International Journal of Heat and Mass Transfer*, Vol. 32, No. 5, 1989, pp. 795–810.

[10]Su, M. H., and Sutton, W. H., "Transient Conductive and Radiative Heat Transfer in a Silica Window," *Journal of Thermophysics and Heat Transfer*, Vol. 9, No. 2, 1995, pp. 370–373.

[11]Abulwafa, E. M., "Conductive–Radiative Heat Transfer in an Inhomogeneous Slab with Directional Reflecting Boundaries," *Journal of Physics D: Applied Physics*, Vol. 32, No. 14, 1999, pp. 1626–1632.

[12]Siegel, R., "Effects of Refractive Index and Diffuse or Specular Boundaries on a Radiating Isothermal Layer," *Journal of Heat Transfer*, Vol. 116, No. 3, 1994, pp. 787–790.

[13]Tsai, C. F., and Nixon, G., "Transient Temperature Distribution of a Multilayer Composite Wall with Effects of Internal Thermal Radiation and Conduction," *Numerical Heat Transfer*, Vol. 10, No. 1, 1986, pp. 95–101.

[14]Timoshenko, V. P., and Trenev, M. G., "A Method for Evaluating Heat Transfer in Multilayered Semitransparent Materials," *Heat Transfer—Soviet Research*, Vol. 18, No. 5, 1986, pp. 44–57.

[15]Hottel, H. C., and Sarofim, A. F., *Radiative Transfer*, McGraw–Hill, New York, 1967, pp. 265, 266.

[16]Tan, H. P., Wang, P. Y., and Xia, X. L., "Transient Coupled Radiation and Conduction in an Absorbing and Scattering Composite Layer," *Journal of Thermophysics and Heat Transfer*, Vol. 14, No. 1, 2000, pp. 77–87.

[17]Wang, P. Y., Tan, H. P., Liu, L. H., and Tong, T. W., "Coupled Radiation and Conduction in a Scattering Composite with Coatings," *Journal of Thermophysics and Heat Transfer*, Vol. 14, No. 4, 2000, pp. 512–522.

[18]Wang, P. Y., Cheng, H. E., and Tan, H. P., "Transient Thermal Analysis of Semitransparent Composite Layer with an Opaque Boundary," *International Journal of Heat and Mass Transfer*, Vol. 45, No. 2, 2001, pp. 425–440.

[19]Tan, H. P., Luo, J. F., and Xia, X. L., "Transient Coupled Radiation and Conduction in a Three-Layer Composite with Semitransparent Specular Interfaces and Surfaces," *Journal of Heat Transfer*, Vol. 124, No. 3, 2002, pp. 470–481.

[20]Luo, J. F., Xia, X. L., Tan, H. P., and Tong, T. W., "Transient Coupled Heat Transfer in Three-Layer Composite with Opaque Specular Surfaces," *Journal of Thermophysics and Heat Transfer*, Vol. 16, No. 3, 2002, pp. 297–305.

[21]Tan, H. P., Tong, T. W., Ruan, L. M., Xia, X. L., and Yu, Q. Z., "Transient Coupled Radiative and Conductive Heat Transfer in an Absorbing, Emitting and Scattering Medium," *International Journal of Heat and Mass Transfer*, Vol. 42, No. 15, 1999, pp. 2967–2980.

[22]Siegel, R., "Two-Flux Green's Function Analysis for Transient Spectral Radiation in a Composite," *Journal of Thermophysics and Heat Transfer*, Vol. 10, No. 4, 1996, pp. 681–688.

[23]Siegel, R., and Howell, J. R., *Thermal Radiation Heat Transfer*, 4th ed., Taylor and Francis, New York, 2002, pp. 80, 81.